Fast-spiking neurons in monkey orbitofrontal cortex underlie economic value computation

Tomoaki Murakawa[1], Takashi Kawai[2], Yuri Imaizumi [3], Hiroshi Yamada[4]*

Short title: Economic value computations in monkey orbitofrontal cortex

1: Academic service office for the medical science area, University of Tsukuba, 1-1-1 Tenno-dai, Tsukuba, Ibaraki 305-8577, Japan

2: The Picower Institute for Learning and Memory, Department of Biology and Department of Brain and Cognitive Sciences, Massachusetts Institute of Technology, Cambridge, MA 02139, USA.

3: College of medical sciences, University of Tsukuba, 1-1-1 Tenno-dai, Tsukuba, Ibaraki 305-8577, Japan

4: Division of Biomedical Science, Institute of Medicine, University of Tsukuba, 1-1-1 Tenno-dai, Tsukuba, Ibaraki 305-8577, Japan.

*Correspondence to Hiroshi Yamada, Ph.D.

Division of Biomedical Science, Institute of Medicine, University of Tsukuba

1-1-1 Tenno-dai, Tsukuba, Ibaraki, 305-8577 Japan

Tel: 81-29-853-6013; e-mail: h-yamada@md.tsukuba.ac.jp

Acknowledgements

The authors express their appreciation to Yoshiko Yabana, Rika Akitake, and Shiho Nishino for their technical assistance. We appreciate Yasuhiro Tsubo for his valuable

comments. Monkey FU was provided by NBRP “Japanese Monkeys” through the National Bio Resource Project of MEXT, Japan. This study was supported by JSPS KAKENHI Grant Number JP:15H05374, 24K02135, JST Moonshot R&D JPMJMS2294 (H.Y.).

Author Contributions

H.Y. designed the study; Y.I. and H.Y. conducted the experiment; T.M., T.K., and H.Y. analyzed the data; H.Y. wrote the manuscript. All authors approved the final manuscript.

Conflict of interest: The authors declare no competing interests.

Data availability: All data used in this study are presented in the manuscript.

Keywords

Orbitofrontal cortex, inhibitory interneuron, monkey, economic behavior

ABSTRACT (149/150)

Inhibitory interneurons are fundamental constituents of cortical circuits that process information to shape economic behaviors. However, the role of inhibitory interneurons in this process remains elusive at the core cortical reward-region, orbitofrontal cortex (OFC). Here, we show that presumed parvalbumin-containing GABAergic interneurons (fast-spiking neurons, FSNs) cooperate with presumed regular-spiking pyramidal neurons (RSNs) during economic-values computation. While monkeys perceived a visual lottery for probability and magnitude of rewards, identified FSNs occupied a small subset of OFC neurons (12%) with high-frequency firing-rates and wide dynamic-ranges, both are key intrinsic cellular characteristics to regulate cortical computation. We found that FSNs showed higher sensitivity to the probability and magnitude of rewards than RSNs. Unambiguously, both neural populations signaled expected values (i.e., probability times magnitude), but FSNs processed these reward's information strongly governed by the dynamic range. Thus, cooperative information processing between FSNs and RSNs provides a common cortical framework for computing economic values.

INTRODUCTION

Activity of inhibitory interneurons regulates information flow in the cortical and subcortical structure (*1-5*). This computational process is thought to rely on circuit structures that regulate the economic behavior of animals. Indeed, cortical inhibitory dysfunction results in various diseases including mental disorders (*6, 7*). Since excitatory neurons constitute the majority of neurons at the core cortical center, the orbitofrontal cortex (OFC), they have been well examined in relation to economic behavior to obtain rewards (*8-14*). However, it remains unclear how OFC inhibitory interneurons are involved in shaping economic behaviors, especially in macaque monkeys, close relatives to humans.

Parvalbumin-containing GABAergic interneurons have been identified as fast-spiking neurons (FSNs) in the brain based on their narrow spike waveform (*15-18*). Although cortical excitatory activity is regulated by inhibitory interneurons (*3, 4, 19-21*), FSN activity in the cortical brain region, especially in monkeys, has only been examined in a small number of studies of cognitive and motor task performance (*1, 22-26*). To our best knowledge, very few studies has examined the role of FSNs in the OFC during economic behavior in both monkeys and rodents. This is largely because FSNs constitute a minority of neurons; thus, only a small amount of sample data can be obtained in a single study. Given this limitation, it is challenging to elucidate the inhibitory mechanism of FSNs at monkey OFC, which process economic-value computations as suspected from the inhibitory dysfunction (*6, 27*).

In the present study, we aimed to understand how FSNs regulate OFC activity during gambling behavior in monkeys. We differentiated FSNs from presumed regular-spiking pyramidal neurons (RSNs) based on spike waveforms recorded extracellularly from the OFC of behaving monkeys. We addressed two critical issues in examining the role of FSNs: 1) How are FSNs in the OFC of behaving monkeys involved in perceiving

expected values, i.e., probability multiplied by magnitude of reward?; 2) How does the activity of FSNs differ from that of RSNs in the OFC when computing expected values? Our results suggest that FSNs compute expected values in coordination with RSNs in the OFC, governed by the dynamic range.

RESULTS

Identification of FSNs and their basic firing properties

We studied total 377 neurons in the OFC of behaving monkeys during a single cue task (Figure 1A). We previously reported monkey behavior during a choice task (*10*) (Figure 1B-D). In short, monkeys chose the option with higher expected value (i.e., probability times magnitude). While the monkeys looked at a visual lottery (Figure 1A), neuronal activity was recorded from the OFC (Figure 1E; medial [mOFC]; 14O, central [cOFC], 13M). We classified the neurons into FSNs and RSNs based on the spike waveforms (Figure 2A), according to the procedure previously used in rat and monkey studies (*2, 19*). A scatter plot of peak width (i.e., width at the half maximum of the negative peak amplitude) against peak-to-valley width (i.e., time from negative peak to valley) for all neurons formed two clusters (Figure 2A). We classified the FSNs as neurons in one cluster that exhibited narrow spike waveforms (Figure 2A, green; see insets). The identified FSNs accounted for approximately 12% (42/377; cOFC, n = 25; mOFC, n= 17) of the recorded OFC neurons. We previously reported the activity of RSNs (*10, 12, 13*) but not the activity of FSNs during the cued lottery task. We note that we did not record the OFC activity during choice task.

Typical FSN activity recorded from the cOFC showed tonic firing of >10 Hz in most of the task periods, with a phasic increase in discharges for some task events (Figure

2B, top). Another example of FSN activity recorded from the mOFC showed a phasic increase in discharges during the start of a trial, and an increase and decrease in activity throughout the trial was observed (Figure 2B, bottom). We first examined these firing rate changes through a trial before and after the visual cue for probability and magnitude appeared (Figure 1A, see gray bars for seven analysis periods). Quantitative comparison of the average firing rates between 42 FSNs and 335 RSNs among seven task periods (Start1, Start2, Cue1, Cue2, Cue3, Cue4, and Pre-fb, see gray bars in Figure 2B) demonstrated higher firing-rates in FSNs than RSNs throughout a task trial (Figure 2C, two-way ANOVA, n = 377, neuron type, $F_{(1,363)} = 97.9$, $P < 0.001$, task period, $F_{(6,363)} = 1.94$, $P = 0.0731$, interaction, $F_{(6,363)} = 1.01$, P = 0.420). Thus, the FSNs identified in the OFC of the behaving monkeys showed a typical characteristic commonly observed in FSNs.

Specifically, FSNs changed their activity at different times during the task trials (Figure 2D). Approximately 60% of FSNs demonstrated peak activity during cue presentation (Figure 2D, top, 59.5%, 25/42), whereas a similar proportion of RSNs showed peak activity during cue presentation (Figure 2E, 44.5%, 149/335, Chi-square test, n = 42, $P = 0.093$, $X^2 = 2.82$, df = 1). Peak activity with short latencies was observed in the FSNs (Figure 2F, latency: Wilcoxon rank-sum test, n = 174, $P < 0.001$, W = 2671.5, df = 1) with higher magnitudes of activity (Figure 2G, peak firing rate: n = 174, $P < 0.001$, W = 896, df = 1). The speed of activity changes were similar between the two types of neurons (Figure 2H, half-peak width: Wilcoxon rank-sum test, n = 174, P = 0.160, W = 2190.5, df = 1). In addition, the dynamic ranges (see Material and Methods) in FSNs were wider than those in RSNs (Figure 2I, n = 377, $P < 0.001$, W = 262337.5, df = 1), which is the critical characteristics to process computation (*28, 29*). We also confirmed that the baseline firing rates during the inter-trial interval were higher in FSNs (Figure 2J,

n = 377, $P < 0.001$, W = 2794, df = 1), similar to activity during the task trials (Figure 2C).

Collectively, high-frequency activity with short latency occurred in FSNs, in contrast to lower firing rates in RSNs. Unambiguously, the dynamic range of FSNs was wider than that of RSNs, indicating that the identified FSNs showed characteristics that matched those of parvalbumin-containing GABAergic interneurons (*30-32*).

Coordinated coding of expected values in FSNs and RSNs

Next, we examined how individual FSNs and RSNs processed the probability and magnitude of rewards during the expected values computation. First, after the cue appearance, 40% to 50% of the FSNs encoded the probability and magnitude of rewards until the outcome appeared (Figure 3A, left). We identified four coding types: probability, magnitude, expected values, and risk-return types. For example, neurons signaling the expected value were found (Figure 3B, see Figure 4E, Cue1), whose activity increased if either probability or magnitude of rewards becomes larger (i.e., EV+ type, see also Figure 3A, reddish). In addition, the probability (Figure 3C, P- type, see also Figure 4E, Cue1 and Figure 3A, bluish) and magnitude (Figure 3D, M+ type, see also Figure 4E, Cue1 and Figure 3A, greenish) types were found for both positive and negative coding type. Indeed, the neural signals carried by FSNs and RSNs were composed of a mixture of these signals (Figure 3A, left and right), such as the signals for the expected value and its components (i.e., probability and magnitude). Thus, Both FSNs and RSNs signal information for the expected value computations.

Next, we compared the encoded information between FSNs and RSNs at the population level. Both neural populations encoded the expected values after cue presentation, as observed in the regression slopes close to 45° angle (Figure 3E, Cue1). This expected value code evolved immediately after the appearance of the cues (Figure

3E, see Cue1, gray line, general linear model, n = 1885, coefficient, $F = 257.6$, $P < 0.001$, df = 1). Thereafter, they gradually lost these expected value signals throughout the trial, as indicated by changes in the regression slopes (Figure 3G, task period, $F = 2.83$, $P = 0.023$, df = 4). The signal change to probability code (regression slop close to 0° angle) occurred concurrently in both types, although the regression slopes were consistently larger in FSNs than in RSNs throughout a trial (cell type, $F = 10.4$, $P = 0.001$, df = 1), indicating FSNs are closer to the expected value code compared to RSNs (i.e., RSNs are closer to probability code). Thus, FSNs and RSNs may share some single computational process at the population level or at the local circuit level, suggesting the existence of common cortical computation in the OFC.

In addition to these comparisons, we compared the amount of carried information in FSNs and RSNs. Carried information by the FSNs was larger compared to RSNs, irrespective of probability or magnitude information (Figure 3F, Four-way ANOVA, n = 1700, neuron type, $F_{(1,1660)} = 229.4$, $P < 0.001$, coding type, $F_{(1,1660)} = 2.23$, $P = 0.135$, task period, $F_{(4,1660)} = 9.51$, $P < 0.001$). Thus, information carried by the FSNs is larger than RSNs, while the carried information changed through a task trial.

Dynamic range and carried information during expected value computation

Finally, we examined how the cortical local circuit structure rely on the expected value computations between FSNs and RSNs. For this purpose, we analyzed the influence of the dynamic range on the extent of carried information by FSNs and RSNs, which is one of the key factors regulating cortical computation according to the local circuit structure (Figure 4A) (*30*). We found that the dynamic range affected amount of carried information in both FSNs and RSNs (Figure 4B, dynamic range, $F = 1109.5$, $P < 0.001$, df = 1). Unambiguously, a wider dynamic range of FSNs co-occurred with stronger neural

modulations, hence larger carried information (Figure. 4B, top) than in RSNs (Figure. 4B, bottom) (cell type, F = 41.6, P < 0.001, df = 1), whereas there was no significant difference between the probability and magnitude information (Fig. 4B, green and blue, coefficient type, F = 2.08, P = 0.150, df = 1). Thus, both FSNs and RSNs process expected value computations under the influence of dynamic range, suggesting the local circuit inhibition (Figure. 4A) may control the computational process.

We also made model selection approach to explore the factors that best explained the encoded information in each of FSNs and RSNs. We found that the combination of the average firing rates in each task period (FR) and the dynamic range (DR) best explained the information processing in both FSNs and RSNs (Figure 4C, see the best model, red) (log-likelihood ratio test, P < 0.001 for all conditions). The same model best explains the amount of carried information in both types. Thus, FSNs and RSNs cooperate in the OFC circuit with the slightly different dynamic range during the expected values computation for economic behavior. We note that the instantaneous firing rate (FR) predominantly affect the amount of the carried information (See Figure 4C, x-label for the selected models in rank order), while coefficient type (CT, i.e., probability or magnitude) only model was the worst one (Worse than null model).

DISCUSSION

In the present study, we analyzed the activity of OFC neurons recorded during economic behavior in monkeys. We differentiated FSNs from other neurons (i.e., RSNs) based on their spike waveforms. Thereafter, we found two properties inherent to FSNs compared to RSNs. First, FSNs displayed high frequency firing rates and wide dynamic range, in contrast to RSNs. Second, the neural representation of the probability and magnitude of

rewards (i.e., carried information for economic behavior) was similar but quantitatively different between the two classes; while FSNs encoded reward information similar to RSNs in terms of the proportion of neurons (Figure 3A) and of the regression coefficient (Figure 3E), signals carried by FSNs were more selective to the probability and magnitude of rewards to signals expected values (Figure 3E and F). Furthermore, we found that dynamic range is a key factor explaining these information processing in both FSNs and RSNs, with a significantly stronger dependence in FSNs on dynamic range (Figure 4B and C). These findings suggest that FSNs regulate information processing to compute expected values in coordination with RSNs via local circuit inhibition during economic behavior in monkeys.

Identification of FSNs with the spike waveform in the primate OFC

In the in vivo cortical structure, FSNs have been identified based on extracellularly recorded spike waveforms in other neurons in rodents (*19*). In Bartho et al., neurons in the rat prefrontal cortex were identified based on a narrow spike waveform recorded extracellularly, which reflects the intracellular properties of the action potential (*33*). Most of the identified neurons showed inhibitory effects on neighboring neurons, while none of these neurons showed excitatory effects (Figure 4 in Bartho et al., 2004), indicating that these narrow spike-waveform neurons were inhibitory interneurons. Accumulating evidence from in vivo and in vitro studies of cortical and subcortical structures supports the hypothesis that narrow spike-waveform neurons are parvalbumin-containing GABAergic interneurons (FSNs) in rodents (*4, 5, 20, 21, 34*) and monkeys (*1, 2, 35*). The electrophysiological and neurochemical properties of the cortical and subcortical structures are similar between primates and rodents (*15, 18*), and it is generally agreed that FSNs recorded from behaving monkeys are parvalbumin-containing GABAergic

interneurons.

In the present study, we identified FSNs based on spike waveforms, similar to previous rodent studies on cortical and subcortical structures (*19, 34*). The identified FSNs exhibited high-frequency firing rates during the task period (approximately 10 Hz) compared to RSNs (Figure 2C). However, the average firing rate of FSNs in this study was lower than that in other monkey's studies in the visual (>30 Hz) (*24*) and prefrontal cortices (>20 Hz) (*36*). This discrepancy may arise from differences in cortical regions as well as behavioral tasks performed by the monkeys, because neural firing rates depend on input to the local circuit (Figure 4A, gray), although cortical areas share a six-layer structure composed of different types of interneurons (*18*).

The spike waveform is one of the predominant characteristics used to identify neuron types in vivo; however, it cannot differentiate between all neuron types. RSNs appear to be comprised of multiple neuron types. In addition, spike waveforms are strongly dependent on the amplifier filter settings: the frequency of the low-pass and high-pass filters and the type of filter (e.g., Butterworth, Bessel, or Chebyshev) (*2*); hence, the characteristics of the spike waveform must be compared in the same experimental settings. Thus, we reliably identified FSNs in the present study.

Dynamic range, firing rates, and information conveyed during economic behavior

In the present study, we found a similar but slightly stronger neural modulation in FSNs than in RSNs at the neuronal population level (Figure 3E-F and Figure 4B). This finding contrasts with that in the striatum, where FSNs are less selective than output neurons (*2*). While the local circuit structures differed between the cortical and subcortical structures (*37-39*), both FSNs in the cortical and subcortical structures consistently showed high-frequency baseline firing rates. The reason for the higher firing rates in

FSNs must be their intrinsic membrane properties of FSNs, such as high input resistance (*30, 32*). If the input resistance is high, the neurons are easy to become active to excitatory inputs. As a result, high-frequency firing rates (Figure 2C and J), and larger changes in task-related activity (Figure 2G), and hence, wider dynamic range (Figure 2I) were observed. These neural properties might be related to the larger changes in carried information as a function of firing rates and dynamic range (Figure 4B, compare FSNs and RSN regression slopes, Figure 4C, red). As a result, the output neurons in cortical (*9, 10, 12, 13*) and subcortical (*40-43*) structures becomes active via feedforward inhibition (Figure 4A) during economic behavior.

We found that relations in reward processing for probability and magnitude were similar between the FSNs and RSNs (Figure 3), but a stronger dependency in FSNs on the dynamic range was observed (Figure 4B). These similarity and difference between FSNs and RSNs should de derived from local circuit structure: mutual inhibition between FSNs and RSNs as well as feedforward inhibition from FSNs to RSNs (Figure 4A, green). The mutual inhibition determines mean firing rates of the circuitry neurons according to the excitatory inputs level, while the feed forward inhibition determines output level of circuit, i.e., RSN's activity. While the excitatory inputs was not able to be observed in this study, these two key properties of local circuit are possible to regulate expected value computations. Indeed recurrent inhibition is known to control circuit dynamics (*44*). Thus, the inhibition of FSNs on RSNs may yield the expected value computation for economic behavior.

Coordinated coding of reward probability and magnitude information by FSNs and RSNs

Our data suggest that FSNs may regulate discharge selectivity of RSNs in the OFC

according to the higher selectivity to the reward information (Figure 3E and F), which was related to the wider dynamic range (Figure 4B). Functional role of the inhibitory interneurons to regulate neural selectivity has been suggested in the cerebral cortex. FSNs with parvalbumin immunoreactivity in visual area V1 of mice have been shown to be selectively involved in shaping orientation tuning and enhancing the directional selectivity of neighboring neurons (*45*). Furthermore, an inhibitory role of FSNs in improving various cognitive functions in distinct cortical regions has been suggested as follows. For example, FSNs in the monkey prefrontal cortex have demonstrated a relationship with the learning and performance of cognitive tasks (*26, 46*). FSNs in visual area V4 showed modulation in their control of attention (*24*), suggesting that the reliability of the output neuron's response is increased by reducing response variability. Thus, feed-forward inhibition (Figure 4A) could be a general mechanism for improving output selectivity, while the input structure is the key factor in driving a local network.

An unambiguous finding of this study was that the coding of the probability and magnitude of rewards by FSNs was similar to that by RSNs (Figure 4). Previous monkey studies of other prefrontal regions have also indicated that FSN activity is selective for reward cues (*25, 36*). Why and how does this coordinated coding of reward information occur in the local circuit (Figure 4A), thereby producing similarities and differences between FSNs and RSNs? If common inputs excite neighboring FSNs and RSNs simultaneously in the cortical circuit (Figure 4A, grays), neural selectivity would be similar. Neighboring RSNs must be suppressed by the inhibition of FSNs (Figure 4A, green), and the balance between excitatory and inhibitory effects must determine neural selectivity for reward information. In contrast, if divergent inputs drive these adjacent cortical neurons, both FSNs and RSNs might sometimes be selective for the probability and magnitude of rewards, but the neural selectivity could be different among these two

neuron types because of the input difference. Further studies are required to elucidate the local circuit dynamics as input–output structures produced by local inhibition in the cortices.

One limitation of our study was that we did not examine the activity of directly connected FSN–RSN pairs. Therefore, we could not directly test the possibilities mentioned above. Previous studies have mostly been performed in the prefrontal cortex, striatum, and hippocampus, but no study has identified FSNs in the monkey OFC, which is involved in economic behavior.

Materials and Methods

Subjects and experimental procedures

Two rhesus monkeys were used in this study (*Macaca mulatta,* SUN, 7.1 kg, male; *Macaca fuscata*, FU, 6.7 kg, female). All experimental procedures were approved by the Animal Care and Use Committee of the University of Tsukuba (protocol no 23-057) and performed in compliance with the US Public Health Service's Guide for the Care and Use of Laboratory Animals. Each animal was implanted with a head restraint prosthesis. Eye movements were measured using a video camera system at 120 Hz. Visual stimuli were generated using a liquid-crystal display at 60 Hz, placed 38 cm from the monkey's face when seated. The subjects performed the cued lottery task 5 days a week. The subjects practiced the cued lottery task for ten months, after which they became proficient in choosing lottery options. We have previously reported the activity of RSNs but have not reported the activity of FSNs during this task.

Behavioral task

Cued lottery tasks. The animals performed one of two visually cued lottery tasks: *single cue task* or *choice task*. Neuronal activity was only recorded during the single cue task. Single cue task: At the beginning of each trial, the monkeys had 2 s to align their gaze within 3˚ of a 1˚-diameter gray central fixation target. After fixating for 1 s, an 8˚ pie chart providing information about the probability and magnitude of the rewards was presented for 2.5 s at the same location as that of the central fixation target. The pie chart was then removed and 0.2 s later, and a 1 kHz and 0.1 kHz tone of 0.15 s duration indicated the reward and no-reward outcomes, respectively. The animals received a fluid reward, for which the magnitude and probability were indicated by green and blue pie charts, respectively; otherwise, no reward was delivered. A high tone preceded the reward by 0.2 s. A low tone indicated that no reward was delivered. An intertrial interval of 4 to 6 s followed each trial.

Choice task: At the beginning of each trial, the monkeys had 2 s to align their gaze within 3˚ of a 1˚-diameter gray central fixation target. After fixing for 1 s, two peripheral 8˚ pie charts providing information on the probability and magnitude of rewards for each of the two target options were presented for 2.5 s, at 8˚ to the left and right of the central fixation location. Gray 1° choice targets appeared at the same locations. After a 0.5 s delay, the fixation target disappeared, cueing saccade initiation. The animals were free to choose for 2 s by shifting their gaze to either target within 3˚ of the choice target. A 1 kHz and 0.1 kHz tone of 0.15 s duration indicated reward and no-reward outcomes, respectively. The animals received a fluid reward, indicated by the green pie chart of the chosen target, with the probability indicated by the blue pie chart; otherwise, no reward was delivered. An intertrial interval of 4 to 6 s followed each trial.

Pay-off and block structure. Green and blue pie charts indicated reward magnitudes from

0.1 to 1.0 mL, in 0.1 mL increments, and reward probabilities from 0.1 to 1.0, in 0.1 increments, respectively. A total of 100 pie charts were used in this study. In the single cue task, each pie chart was presented once in random order. In the choice task, two pie charts were randomly assigned to the two options. During one session of electrophysiological recording, approximately 30 to 60 trial blocks of the choice task were sometimes interleaved with 100 to 120 trial blocks of the single cue task.

Calibration of the reward supply system. A precise amount of liquid reward was controlled and delivered to the monkeys using a solenoid valve. An 18-gauge tube (0.9 mm inner diameter) was attached to the tip of the delivery tube to reduce variation across trials. The reward amount in each payoff condition was calibrated by measuring the weight of water with a precision of 0.002 g (2 μL) on a single-trial basis. This calibration method was the same as that described previously (*9*).

Electrophysiological recordings

Conventional techniques were used to record single-neuron activity in the cOFC and mOFC. Monkeys were implanted with recording chambers (28 mm × 32 mm) targeting the OFC and striatum, centered 28 mm anterior to the stereotaxic coordinates. The locations of the chambers were verified using anatomical magnetic resonance imaging (MRI). At the beginning of the daily recording sessions, a stainless-steel guide tube was placed within a 1-mm spacing grid, and a tungsten microelectrode (1-3 MΩ, FHC) was passed through the guide tube. To record neurons in the mOFC and cOFC, the electrode was lowered until it approximated the bottom of the brain after passing through the cingulate cortex, dorsolateral prefrontal cortex, or between them. Electrophysiological signals were amplified, bandpass filtered, and monitored. Single-neuron activity was

isolated based on spike waveforms. We recorded from the two brain regions of a single hemisphere of each of the two monkeys (179 in monkey SUN and 198 in monkey FU): 42 SFNs (cOFC, 25, mOFC, 17), and 335 RSNs (cOFC, 182, mOFC, 153) for FSNs and RSNs. The activity of all individual neurons was sampled when the activity of an isolated neuron demonstrated a good signal-to-noise ratio (>2.5). Blinding was not performed. The sample sizes required to detect effect sizes (number of recorded neurons, number of recorded trials in a single neuron, and number of monkeys) were estimated according to previous studies (*9, 40, 47, 48*). Neural activity was recorded during 100-120 trials of the single cue task. During the choice trials, neural activity was not recorded.

Classification of neuron type.

In the analysis, FSNs (presumed to be parvalbumin-containing GABAergic interneurons) were differentiated from RSNs (presumed to be pyramidal neurons) by their spike width (i.e., the width at the half maximum of the negative peak amplitude and the width of the spike from peak to valley), according to a previous study (*19*). We classified the FSNs as neurons in one cluster that exhibited narrow spike waveforms. In our previous reports (*10, 12, 13, 43*), we reported the activity of RSNs but not of FSNs. The number of reported RSNs in this study differed from that in previous studies because we did not perform a quantitative classification of these neurons based on the waveform in those studies.

Statistical analysis

Statistical analyses were performed using the R statistical software package (http://www.r-project.org/). All statistical tests for behavioral and neural analyses were two-tailed.

Effects of units on statistical analysis. In the present study, we used two variables for analysis: probability and magnitude. We defined the probability of the reward from 0.1 to 1.0, and the magnitude of the reward from 0.1 to 1.0 mL. Under this unit definition, the effects of probability and magnitude on the data were equivalent.

Behavioral analysis

No new behavioral results were included; however, the procedure for the behavioral analysis was as follows:

We previously reported that monkey behavior depends on expected values defined as the probability time magnitude (*10*). We described the analysis steps to check whether the monkey's behavior reflected task parameters, such as reward probability and magnitude. Importantly, we showed that the monkeys' choice behavior reflected the expected values of the rewards, i.e., the probability multiplied by the magnitude. For this purpose, the percentage choosing the right option was analyzed in the pooled data using a general linear model with a binomial distribution:

$$Pchooses_R = 1 / (1 + e^{-z}) \quad (3)$$

where the relationship between $Pchooses_R$ and Z is given by the logistic function in each of the following three models: number of pie segments (M1), probability and magnitude (M2), and expected values (M3).

$$\text{M1: } Z = b_0 + b_1 Npie_L + b_2 Npie_R \quad (4)$$

where b_0 is the intercept, and $Npie_L$ and $Npie_R$ are the number of pie segments contained in the left and right pie chart stimuli, respectively. The values of b_0 to b_2 are free parameters and were estimated by maximizing the log likelihood.

$$\text{M2: } Z = b_0 + b_1 P_L + b_2 P_R + b_3 M_L + b_4 M_R \quad (5)$$

where b_0 is the intercept; P_L and P_R are the probabilities of rewards for the left and right pie chart stimuli, respectively; and M_L and M_R are the magnitudes of rewards for the left and right pie chart stimuli, respectively. The values of b_0 to b_4 are free parameters and are estimated by maximizing the log likelihood.

$$\text{M3: } Z = b_0 + b_1 EV_L + b_2 EV_R \qquad (6)$$

where b_0 is the intercept and EV_L and EV_R are the expected values of rewards as probability multiplied by magnitude for the left and right pie chart stimuli, respectively. The values of b_0 to b_2 are free parameters and were estimated by maximizing the log likelihood. We identified the best model to describe the monkeys' behavior by comparing their goodness-of-fit based on Akaike's information criterion (AIC) and Bayesian information criterion (BIC) (*49*).

Neural analysis.

Peri-stimulus time histograms were drawn for each single neuron activity aligned at the onset of a visual cue. The average activity curves were smoothed using a 50-ms Gaussian kernel (σ = 50 ms). We analyzed neural activity during a 2.5-s period of pie chart stimulus presentation in the single cue task, including baseline activity before the presentation of cues during a 1.0 s fixation period. The firing rates of each neuron during the 0.5 s time window were estimated every 0.5 s for a total of seven analysis periods named Start1, Start2, Cue1, Cue2, Cue3, Cue4, and Pre-fb (feedback). A Gaussian kernel was not used for statistical analyses.

Basic firing properties, such as peak firing rates, peak latency, duration of peak activity (half-peak width), and dynamic range, were compared among the four brain regions using parametric or nonparametric tests, with a statistical significance level of $P < 0.05$. The dynamic range (DR) was defined as the firing rate difference between the

maximum and minimum among the seven task periods after cue presentation: Start1, Start2, Cue1, Cue2, Cue3, Cue4, and Pre-fb. Baseline firing rates 1 s before the appearance of the central fixation targets were also compared, with a statistical significance level of $P < 0.05$. Yamada et al. (2021) also analyzed the basic firing properties of RSNs, but not for FSNs.

Linear regression to detect firing modulations in each individual neuron. Neural discharge rates (F) were fitted using the following variables:

$$F = b_0 + b_p \,\text{Probability} + b_m \,\text{Magnitude} \qquad (8)$$

where Probability and Magnitude are the probability and magnitude of the rewards indicated by the pie chart, respectively. b_0 is the intercept. If b_p and b_m are not zero at $P < 0.05$, the discharge rates were regarded as being significantly modulated by that variable.

On the basis of the linear regression, activity modulation patterns were categorized into several types: “Probability” (P) type with a significant b_p and without a significant b_m; “Magnitude” (M) type without a significant b_p and with a significant b_m; “Expected value” (EV) type with significant b_p and b_m with the same sign (i.e., positive b_p and positive b_m or negative b_p and negative b_m); “Risk-Return” (RR) type with significant b_p and b_m with both having opposite signs (i.e., negative b_p and positive b_m or positive b_p and negative b_m) and “non-modulated” type without significant b_p and b_m. The risk–return types reflect high-risk high returns (prefer low probability and large magnitude) or low-risk low returns (prefer high probability and low magnitude).

We compared the basic firing properties and activity modulations between the FSNs and RSNs as follows: 1) proportion of neuron types using the chi-square test; 2) average firing rates using ANOVA, Kruskal-Wallis test, or Wilcoxon rank-sum test with Bonferroni

correction for multiple comparisons; and 3) regression coefficients using a general linear model, such as ANOVA and linear regression.

Linear regression to detect firing modulations at the level of population. The regression coefficients for reward magnitude (*R*) were fitted using the following variables:

$$R = b_0 + b_1 R_p + b_2 \text{ Task period} + b_3 \text{ Cell type} \quad (9)$$

where R_p denotes the regression coefficient of the reward probability. Task period was a categorical variable composed of Cue1, Cue2, Cue3, Cue4, and Pre-fb. Cell type is a categorical variable comprising FSNs and RSNs. If b_1 to b_3 are not zero at $P < 0.05$, the discharge rates were regarded as being significantly modulated by that variable.

Dynamic range and neural modulations. To analyze the influence of basic firing properties on the regression coefficients for the probability and magnitude of rewards, we modeled how the dynamic range and average firing rates affect neural modulation as follows:

$$R = b_0 + b_1 DR + b_2 FR + b_3 CT \quad (10)$$

Where *R* is the absolute value of the regression coefficients for the probability and magnitude of the rewards, b_p and b_m in Eq. 8. b_0 is the intercept. *DR* is the dynamic range. *FR* is the average firing rates in each of the five task periods after cue presentation: Cue1, Cue2, Cue3, Cue4, and Pre-fb. *CT* is the regression coefficient type (i.e., probability or magnitude) as a categorical parameter. If b_1 is not 0 at $P < 0.05$, neural modulation by the probability and magnitude of rewards was regarded as significantly affected by the dynamic range of neurons. If b_2 is not 0 at $P < 0.05$, neural modulation by the probability and magnitude of rewards was regarded as significantly affected by the average firing rate in each neuron. If b_3 is not 0 at $P < 0.05$, neural modulations by the probability and

magnitude of rewards were different among the probability and magnitude of rewards, i.e., the regression coefficient types.

Model comparisons. To identify the best structural model to describe neural modulation, as described above, we applied a model selection approach based on all possible combinations of variables in Eq. 10. We sought a combination of best-fit parameters to explain the neural modulation based on the probability and magnitude of rewards. We compared the goodness of fit based on AIC and BIC (*49*).

$$\mathrm{AIC\ (Model)} = -2L + 2k \qquad (10)$$

$$\mathrm{BIC\ (Model)} = -2L + k \log n \qquad (11)$$

where, L is the maximum log-likelihood of the model, k is the number of free parameters, and n is the sample size. After estimating the best-fit parameters for each model, the model that exhibited the smallest AIC and BIC values was selected. To evaluate the model fit, we estimated the difference between these values and the null model's AIC or BIC, which is the log likelihood under the assumption that all free parameters are zero in the model, except the intercept, b_0. We used the log-likelihood ratio test for each of the selected models to the null model at $P < 0.05$.

REFERENCES

1. G. Gonzalez-Burgos, L. S. Krimer, N. V. Povysheva, G. Barrionuevo, D. A. Lewis, Functional properties of fast spiking interneurons and their synaptic connections with pyramidal cells in primate dorsolateral prefrontal cortex. *J Neurophysiol* **93**, 942-953 (2005).
2. H. Yamada *et al.*, Characteristics of fast-spiking neurons in the striatum of

behaving monkeys. *Neurosci Res* **105**, 2-18 (2016).

3. R. Wilbers *et al.*, Structural and functional specializations of human fast-spiking neurons support fast cortical signaling. *Sci Adv* **9**, eadf0708 (2023).
4. N. Giordano *et al.*, Fast-Spiking Interneurons of the Premotor Cortex Contribute to Initiation and Execution of Spontaneous Actions. *J Neurosci* **43**, 4234-4250 (2023).
5. S. Chamberland *et al.*, Brief synaptic inhibition persistently interrupts firing of fast-spiking interneurons. *Neuron* **111**, 1264-1281 e1265 (2023).
6. R. Hattori, K. V. Kuchibhotla, R. C. Froemke, T. Komiyama, Functions and dysfunctions of neocortical inhibitory neuron subtypes. *Nat Neurosci* **20**, 1199-1208 (2017).
7. P. Allami, N. Yazdanpanah, N. Rezaei, The role of neuroinflammation in PV interneuron impairments in brain networks; implications for cognitive disorders. *Rev Neurosci*, (2025).
8. E. L. Rich, J. D. Wallis, Decoding subjective decisions from orbitofrontal cortex. *Nat Neurosci* **19**, 973-980 (2016).
9. H. Yamada, K. Louie, A. Tymula, P. W. Glimcher, Free choice shapes normalized value signals in medial orbitofrontal cortex. *Nat Commun* **9**, 162 (2018).
10. H. Yamada, Y. Imaizumi, M. Matsumoto, Neural Population Dynamics Underlying Expected Value Computation. *J Neurosci* **41**, 1684-1698 (2021).
11. A. Pastor-Bernier, A. Stasiak, W. Schultz, Reward-specific satiety affects subjective value signals in orbitofrontal cortex during multicomponent economic choice. *Proc Natl Acad Sci U S A* **118**, (2021).
12. Y. Imaizumi, A. Tymula, Y. Tsubo, M. Matsumoto, H. Yamada, A neuronal

prospect theory model in the brain reward circuitry. *Nat Commun* **13**, 5855 (2022).

13. H. Chen *et al.*, Stable Neural Population Dynamics in the Regression Subspace for Continuous and Categorical Task Parameters in Monkeys. *eNeuro* **10**, (2023).
14. C. Padoa-Schioppa, Neuronal origins of choice variability in economic decisions. *Neuron* **80**, 1322-1336 (2013).
15. Y. Kawaguchi, C. J. Wilson, S. J. Augood, P. C. Emson, Striatal interneurones: chemical, physiological and morphological characterization [published erratum appears in Trends Neurosci 1996 Apr;19(4):143]. *Trends Neurosci* **18**, 527-535 (1995).
16. B. Cauli *et al.*, Molecular and physiological diversity of cortical nonpyramidal cells. *J Neurosci* **17**, 3894-3906 (1997).
17. J. DeFelipe, Types of neurons, synaptic connections and chemical characteristics of cells immunoreactive for calbindin-D28K, parvalbumin and calretinin in the neocortex. *J Chem Neuroanat* **14**, 1-19 (1997).
18. Y. Kawaguchi, S. Kondo, Parvalbumin, somatostatin and cholecystokinin as chemical markers for specific GABAergic interneuron types in the rat frontal cortex. *J Neurocytol* **31**, 277-287 (2002).
19. P. Bartho *et al.*, Characterization of neocortical principal cells and interneurons by network interactions and extracellular features. *J Neurophysiol* **92**, 600-608 (2004).
20. S. F. Owen, J. D. Berke, A. C. Kreitzer, Fast-Spiking Interneurons Supply Feedforward Control of Bursting, Calcium, and Plasticity for Efficient Learning. *Cell* **172**, 683-695 e615 (2018).

21. R. J. Hatch, G. D. C. Mendis, K. Kaila, C. A. Reid, S. Petrou, Gap Junctions Link Regular-Spiking and Fast-Spiking Interneurons in Layer 5 Somatosensory Cortex. *Front Cell Neurosci* **11**, 204 (2017).

22. B. Wang *et al.*, Firing Frequency Maxima of Fast-Spiking Neurons in Human, Monkey, and Mouse Neocortex. *Front Cell Neurosci* **10**, 239 (2016).

23. N. V. Povysheva *et al.*, Properties of excitatory synaptic responses in fast-spiking interneurons and pyramidal cells from monkey and rat prefrontal cortex. *Cereb Cortex* **16**, 541-552 (2006).

24. J. F. Mitchell, K. A. Sundberg, J. H. Reynolds, Differential attention-dependent response modulation across cell classes in macaque visual area V4. *Neuron* **55**, 131-141 (2007).

25. T. Kawai, H. Yamada, N. Sato, M. Takada, M. Matsumoto, Preferential Representation of Past Outcome Information and Future Choice Behavior by Putative Inhibitory Interneurons Rather Than Putative Pyramidal Neurons in the Primate Dorsal Anterior Cingulate Cortex. *Cereb Cortex* **29**, 2339-2352 (2019).

26. C. Constantinidis, P. S. Goldman-Rakic, Correlated discharges among putative pyramidal neurons and interneurons in the primate prefrontal cortex. *J Neurophysiol* **88**, 3487-3497 (2002).

27. T. Prevot, E. Sibille, Altered GABA-mediated information processing and cognitive dysfunctions in depression and other brain disorders. *Mol Psychiatry* **26**, 151-167 (2021).

28. H. Zhang *et al.*, Neural-WDRC: A Deep Learning Wide Dynamic Range Compression Method Combined With Controllable Noise Reduction for Hearing Aids. *Trends Hear* **29**, 23312165241309301 (2025).

29. W. L. Shew, H. Yang, T. Petermann, R. Roy, D. Plenz, Neuronal avalanches imply maximum dynamic range in cortical networks at criticality. *J Neurosci* **29**, 15595-15600 (2009).

30. Y. Kawaguchi, Physiological subgroups of nonpyramidal cells with specific morphological characteristics in layer II/III of rat frontal cortex. *J Neurosci* **15**, 2638-2655 (1995).

31. N. V. Povysheva *et al.*, Parvalbumin-positive basket interneurons in monkey and rat prefrontal cortex. *J Neurophysiol* **100**, 2348-2360 (2008).

32. Y. Kawaguchi, Physiological, morphological, and histochemical characterization of three classes of interneurons in rat neostriatum. *J Neurosci* **13**, 4908-4923 (1993).

33. D. A. Henze *et al.*, Intracellular features predicted by extracellular recordings in the hippocampus in vivo. *J Neurophysiol* **84**, 390-400 (2000).

34. G. J. Gage, C. R. Stoetzner, A. B. Wiltschko, J. D. Berke, Selective activation of striatal fast-spiking interneurons during choice execution. *Neuron* **67**, 466-479 (2010).

35. J. Kunimatsu, S. Yamamoto, K. Maeda, O. Hikosaka, Environment-based object values learned by local network in the striatum tail. *Proc Natl Acad Sci U S A* **118**, (2021).

36. H. Fan, X. Pan, R. Wang, M. Sakagami, Differences in reward processing between putative cell types in primate prefrontal cortex. *PLoS One* **12**, e0189771 (2017).

37. H. Inokawa, N. Matsumoto, M. Kimura, H. Yamada, Tonically Active Neurons in the Monkey Dorsal Striatum Signal Outcome Feedback during Trial-and-error Search Behavior. *Neuroscience* **446**, 271-284 (2020).

38. Y. Tsubo, Y. Isomura, T. Fukai, Neural dynamics and information representation in microcircuits of motor cortex. *Front Neural Circuits* **7**, 85 (2013).

39. Y. Isomura, R. Harukuni, T. Takekawa, H. Aizawa, T. Fukai, Microcircuitry coordination of cortical motor information in self-initiation of voluntary movements. *Nat Neurosci* **12**, 1586-1593 (2009).

40. H. Yamada *et al.*, Coding of the long-term value of multiple future rewards in the primate striatum. *J Neurophysiol* **109**, 1140-1151 (2013).

41. H. Yamada, H. Inokawa, N. Matsumoto, Y. Ueda, M. Kimura, Neuronal basis for evaluating selected action in the primate striatum. *Eur J Neurosci* **34**, 489-506 (2011).

42. H. Yamada, N. Matsumoto, M. Kimura, History- and current instruction-based coding of forthcoming behavioral outcomes in the striatum. *J Neurophysiol* **98**, 3557-3567 (2007).

43. H. Chen *et al.*, Formation of brain-wide neural geometry during visual item recognition in monkeys. *iScience* **28**, 111936 (2025).

44. M. B. Lynn *et al.*, Nonlinear recurrent inhibition through facilitating serotonin release in the raphe. *Nat Neurosci*, (2025).

45. S. H. Lee *et al.*, Activation of specific interneurons improves V1 feature selectivity and visual perception. *Nature* **488**, 379-383 (2012).

46. X. L. Qi, C. Constantinidis, Correlated discharges in the primate prefrontal cortex before and after working memory training. *Eur J Neurosci* **36**, 3538-3548 (2012).

47. H. Yamada, N. Matsumoto, M. Kimura, Tonically active neurons in the primate caudate nucleus and putamen differentially encode instructed

motivational outcomes of action. *J Neurosci* **24**, 3500-3510 (2004).

48. K. Enomoto, N. Matsumoto, H. Inokawa, M. Kimura, H. Yamada, Topographic distinction in long-term value signals between presumed dopamine neurons and presumed striatal projection neurons in behaving monkeys. *Sci Rep* **10**, 8912 (2020).

49. K. Burnham, D. Anderson, Multimodel inference: understanding AIC and BIC in model selection. *Sociol. Method Res.* **33**, 261–304 (2004).

Figures

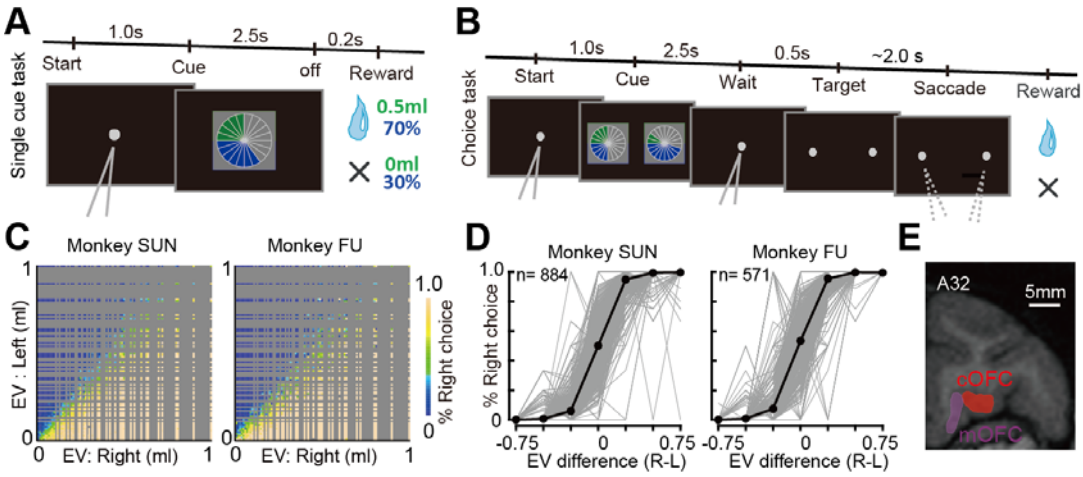

Figure 1. Task, behavior, and recording sites.

A Sequence of events during the single cue task. A single pie chart with green and blue segments was presented visually to the monkeys. **B** Choice task. Two pie charts were presented visually to the monkeys on the left and right sides of the center. After visual fixation on the central point, it disappeared, and the monkeys chose either of the targets by fixating on it. A block of choice trials was sometimes interleaved between the single cue trial blocks. During the choice trials, neural activity was not recorded. **C** Percentages of right target choices during the choice task plotted against the expected values (EVs) of the left and right target options. Aggregated choice data were used. **D** Percentage of right target choices estimated in each recording session (gray lines) plotted against the difference in expected values (right minus left). The choice data were segmented by seven conditions of the difference in the expected values: -1.0 ~ -0.5, -0.5 ~ -0.3, -0.3 ~ -0.1, -0.1 ~ 0.1, 0.1 ~ 0.3, 0.3 ~ 0.5, and 0.5 ~1.0. The black plots indicate the mean values. **E** Illustration of neural recording areas based on sagittal MR Neurons were recorded from the medial (mOFC, 14O, orbital part of area 14) and central parts of the orbitofrontal cortex (cOFC, 13M, medial part of area 13) at the A31-A34 anterior-posterior (A-P) level. These figures are taken from Yamada et al. (2021).

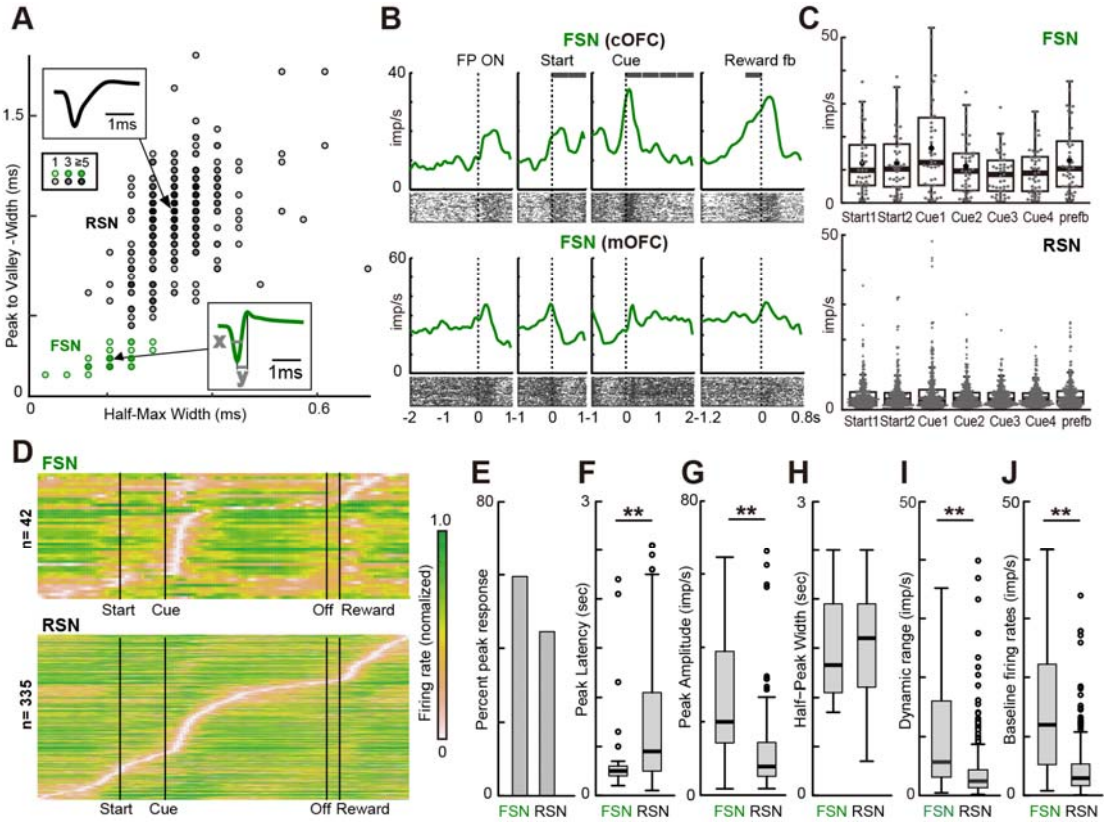

Figure 2. Classification of FSNs and their basic activity properties during task trials.

A Scatter plots of mean spike waveform durations (x, width at the half maximum of the negative peak amplitude; y, width from peak to valley; see inset) for OFC neurons. FSNs were defined as neurons in one cluster that exhibited narrow spike waveforms (green). Neurons in clusters with wider spike waveforms were classified as RSNs. **B** Two examples of FSN activity recorded from the cOFC of monkey SUN and the mOFC of monkey FU during the single cue task. Rasters and histograms were aligned for each behavioral event. The seven gray bars indicate the 0.5 s analysis periods. All histograms (50-ms bins) were smoothed using a Gaussian kernel (50 ms). **C** Average firing rates of 42 FSNs and 335 RSNs during seven analysis periods. **D** Color map histograms of FSN and RSN activity. Each horizontal line indicates the neural activity aligned with cue onset averaged for all lottery conditions. Neuronal firing rates were normalized to peak activity. **E** Percentage of neurons showing an activity peak during cue presentation. **F** Peak activity latency after cue

presentation. **G** Firing rates of peak activity observed during cue presentation. **H** Half-peak width, indicating the phasic nature of activity changes. **I** Dynamic range defined as the difference between maximum and minimum firing rates. **J** Box plots of baseline firing rates during the 1 s time period before the presentation of the central fixation target. In **E-J**, asterisks indicate statistical significance between the two neural populations (Wilcoxon rank-sum test, *$P < 0.05$, **$P < 0.01$).

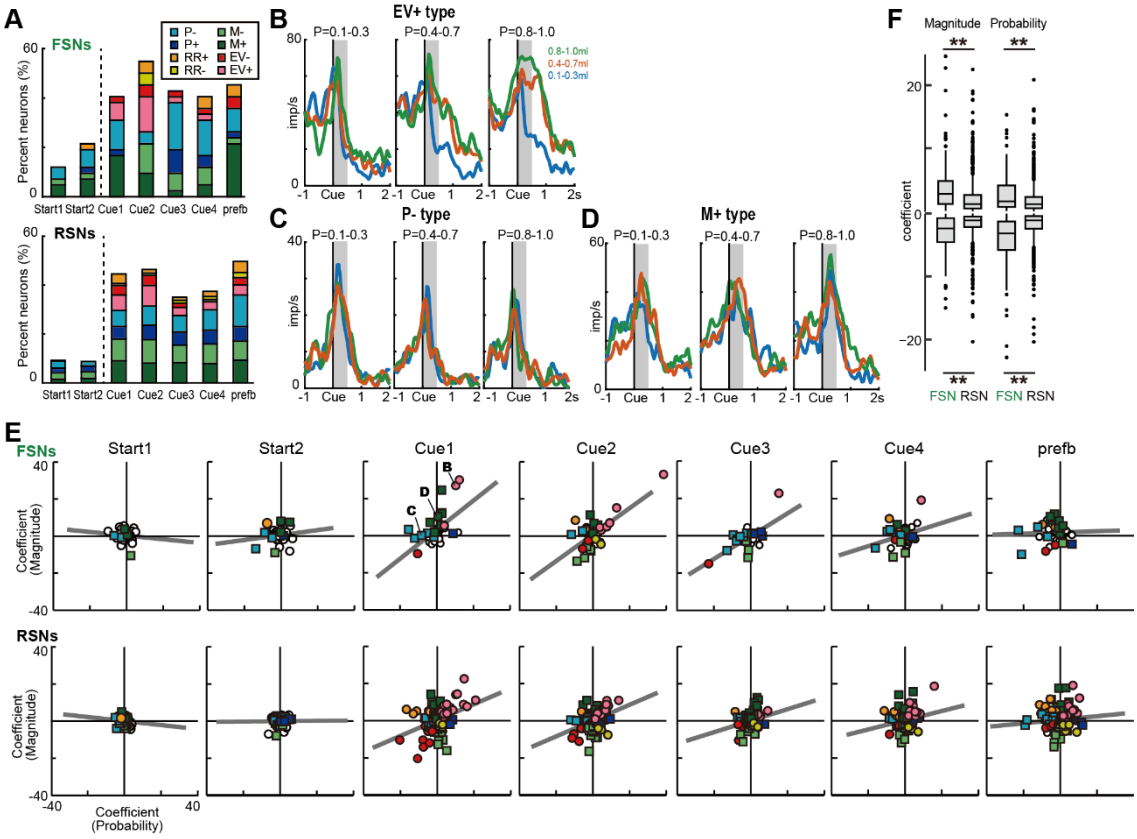

Figure 3. Probability and magnitude modulations in FSNs and RSNs.

A Percentages of neural modulation types for FSNs and RSNs during the seven analysis periods. Probability (P), magnitude (M), expected value (EV), and risk–return (RR) types were detected based on the significance of the positive and negative regression coefficients. **B-D** Examples of FSNs for EV+, M+, and P- are shown. Reward probability (P) is differentiated among low, middle, and high conditions. Reward magnitude is also differentiated among low, middle, and high conditions. The gray-hatched time windows are the analysis periods, Cue1. **E** Regression coefficients for the probability and magnitude of rewards during a task trial. The gray lines indicate the regression slopes. **F** Box plots of the regression coefficient for the probability and magnitude of rewards among positive- and negative-coding type. Asterisks indicate statistical significance between the two neural populations (Wilcoxon rank-sum test, *P < 0.05, **P < 0.01).

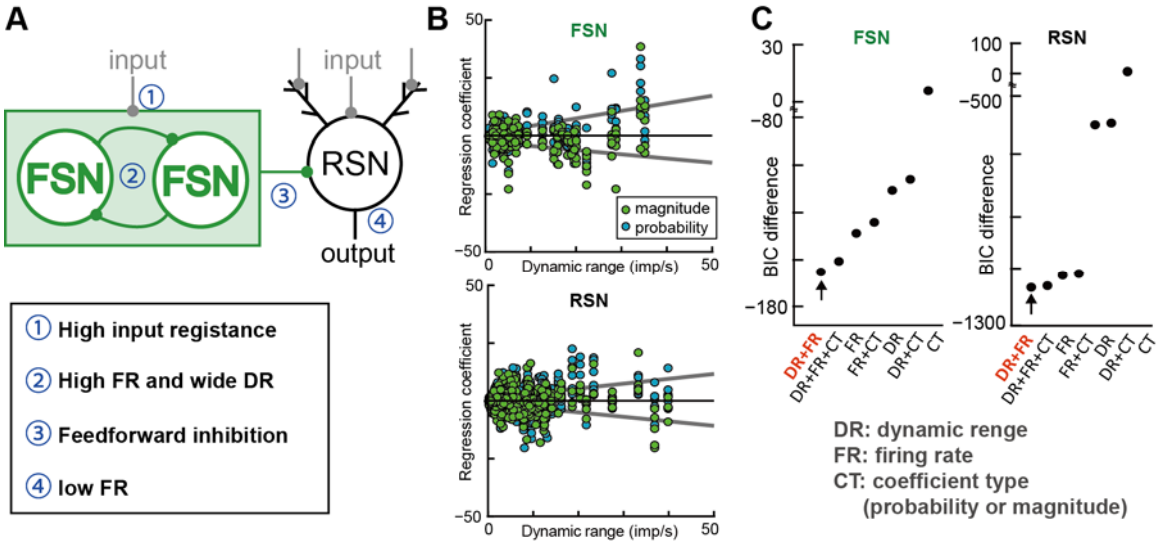

Figure 4. Dynamic rage of firing rates differed between FSN and RSN in neural modulation.

A Schematic depiction of the cortical circuit for the presumed parvalbumin-containing GABAergic interneurons (FSN) and the presumed output pyramidal neurons (RSN). Below indicates information processing via inhibition is shown from 1 to 4. **B** Plots of regression coefficients for probability (blue) and magnitude (green) of rewards against dynamic range for FSNs (left) and RSNs (right). Gray lines show the regression slopes from the general linear model. **C** Plots of the difference in Bayesian information criterion values between the top seven models and the null model. The X-axis labels indicate the selected models in rank order. In A and B, DR, dynamic range; FR, firing rate; CT, regression coefficient type (i.e., probability or magnitude). In B, red indicate the best model.